International Journal of Heat and Technology
Vol. 41, No. 3, June, 2023, pp. 730-736
Journal homepage: http://iieta.org/journals/ijht

Effects of Surface Roughness and MHD on Squeeze Film Characteristics for Various Finite Porous Plate Geometries with Couple-Stress Fluid

Faizan Ahmed Masood, Sujatha Elamparithi*

Department of Mathematics, College of Engineering and Technology, SRM Institute of Science and Technology, Kattankulathur 603203, India

Corresponding Author Email: sujathae@srmist.edu.in

https://doi.org/10.18280/ijht.410328

Received: 28 February 2023
Accepted: 16 June 2023

Keywords:
couple-stress fluid, MHD, porosity, surface roughness

ABSTRACT

This article examines the performance of squeeze film properties in various finite plates lubricated with couple-stress fluid and subjected to a transverse magnetic field and surface roughness. On the basis of Stokes couple-stress fluid theory and Christensen's stochastic model are used to derive a modified Reynolds equation. The squeeze film pressure and workload were calculated using the resultant equation with boundary conditions. The study found that the bearing systems with surface roughness performed better than those with a smooth surface when a magnetic field was present. Additionally, the presence of viscosity variation resulted in a significant increase in the workload of finite plates compared to non-viscosity variation cases. The study also revealed that the load was reduced in the presence of porosity compared to the non-porous case.

1. INTRODUCTION

The use of a non-Newtonian fluid as a lubricant has piqued the curiosity of many researchers due to the increased use of non-Newtonian fluids in contemporary technology. Ariman et al. [1, 2] and Stokes [3] developed several microcontinuum models to describe the flow behaviour of various types of non-Newtonian lubricants. The performance of different bearing systems has been widely studied using Stokes' microcontinuum theory. Couple-stresses have an impact on this performance. The use of couple-stresses leads to a greater workload and a longer response time, as shown by Lin [4], Naduvinamani et al. [5], Naduvinamani and Patil [6], Ramanaiah [7] and Bujurke and Jayaraman [8], among others.

Magnetohydrodynamics (MHD) is a field of study that explores the interaction between conducting fluids and electromagnetic phenomena. The existence of a magnetic field plays a significant role in influencing and controlling tribological properties. Bearings that utilize conducting fluids in MHD exhibit exceptional properties such as high thermal conductivity and electrical conductivity, which outperform traditional bearings.

Surface roughness has typically had a direct impact on solid thin film electrical, optical, and mechanical devices. Any solid material's surface roughness will have a significant impact on the analysis of the macroscopic contact angle on its flat surface, which is crucial for many processes including lubricating, spreading, and wetting. Many techniques have been used to examine the effects of rough surfaces, Tzeng and Saibel [9] and Christensen [10] both used stochastic approaches and stochastic theories to slider bearing. Christensen and Tonder [11-13] examined the effects of roughness on slider and journal bearings, whereas Naduvinamani et al. [14] investigated a sphere and flat plate, and Rajani et al. [15] employed conical bearings. Based on their study, it has been concluded that surface roughness increases squeeze film pressure, squeeze film load capacity, and squeeze film approach time.

In practice, assuming a constant viscosity for the lubricant under consideration is a generalization. In this problem the viscosity of lubricants is not constant throughout their entire height, and it can vary with the operating temperature. Therefore, to account for the change in viscosity with temperature, an empirical relation of the form is used [16].

$$\mu = \mu_1 \left(\frac{h}{h_0}\right)^Q$$

The parameter μ_1 represents the known viscosity at the minimum film thickness $h = h_0$. The variable Q, which takes on values between 0 and 1 depending on the lubricant properties, is used in the equation; Q equals 0 for perfect Newtonian fluids and 1 for perfect gases. The situation being analyzed assumes the presence of thermal equilibrium.

In the current work, the effects of surface roughness and hydro-magnetic interactions on the couple-stress fluid squeeze film between different finite plates are investigated. Non-Newtonian hydro-magnetic Reynolds equation is produced by using the stochastic model of Christensen and Stokes microcontinuum theory and the hydro-magnetic flow theory, considering the lubricant to be of the form of a very thin film. The impacts of surface roughness, hydromagnetic aspect and couple-stress fluids with viscosity variation are studied via the variation of the Hartmann parameter M, couple-stress parameter l^*, viscosity variation parameter Q and permeability parameter Ψ.

2. MATHEMATICAL FORMULATION

Figure 1 displays the configuration of distinct finite plates.

The lubricant that is taken into account within the film area is a couple-stress fluid. The upper plate moves towards the lower plate at a uniform velocity, represented by $v = \frac{dh}{dt}$. The lower surface is considered to be both porous and rough, with asperities contributing to the roughness of the surface. This roughness can be expressed mathematically as follows,

$$H = h(t) + h_s(x, y, \zeta)$$

where, the first half of the above expression represents the deterministic part of the film thickness and the second half stands for the random part of the film thickness. ζ is the index parameter which determines exact roughness pattern.

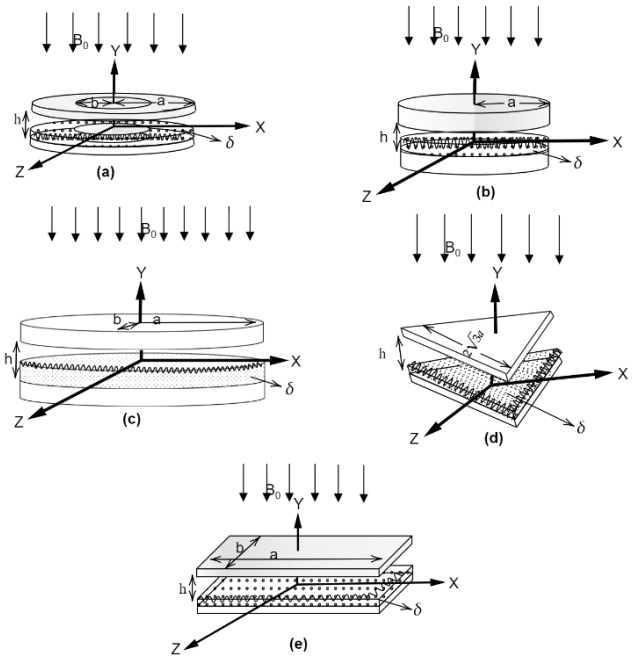

Figure 1. Different geometries (a) Annular, (b) Circular, (c) Elliptic, (d) Triangular, (e) Rectangular

The expression defines the expectancy operator, denoted by $E(\star)$

$$E(\star) = \int_{-\infty}^{\infty} (\star) f(h_s) ds$$

The equation expresses the probability density function $f(h_s)$ of the stochastic variable h_s, which is used in the calculation of the expectancy operator.

$$f(h_s) = \begin{cases} \frac{35}{32c^7}\,(c^2 - h_s^2)^3 & -c \le h_s \le c \\ 0 & otherwise \end{cases}$$

The Stokes equations for continuity and momentum for the couple-stress fluid may be formulated as follows, assuming the fundamental hypotheses of hydrodynamic lubrication of thin films as stated in Fathima [17],

$$\mu \frac{\partial^2 u}{\partial y^2} - \eta \frac{\partial^4 u}{\partial y^4} - \frac{\sigma B_0^2}{\mu} u - \frac{\partial p}{\partial x} = 0 \tag{1}$$

$$\mu \frac{\partial^2 w}{\partial y^2} - \eta \frac{\partial^4 w}{\partial y^4} - \frac{\sigma B_0^2}{\mu} w - \frac{\partial p}{\partial z} = 0 \tag{2}$$

$$\frac{\partial p}{\partial y} = 0 \tag{3}$$

$$\frac{\partial u}{\partial x} + \frac{\partial v}{\partial y} + \frac{\partial w}{\partial z} = 0 \tag{4}$$

The following equation describe the boundary conditions for the problem being considered.

(i) At the lower plate (y=0)

$$u = w = 0, \frac{\partial^2 u}{\partial y^2} = \frac{\partial^2 w}{\partial y^2} = 0, v = -v^\star \tag{5}$$

(ii) At the upper plate (y=h)

$$u = w = 0, \frac{\partial^2 u}{\partial y^2} = \frac{\partial^2 w}{\partial y^2} = 0, v = \frac{dh}{dt} \tag{6}$$

Within the porous matrix, the velocity component in the y-direction, denoted by $v^\star$, is subject to a modified Darcy's law and is given by:

$$v^\star = \frac{-k}{\mu(1-\beta)} \frac{\partial p^\star}{\partial y}$$

where, $p^\star$ represents the pressure in the porous medium, k is the permeability of porous matrix and β denotes the ratio of micro-structure size to the pore size.

The Laplace equation is satisfied by the pressure with in porous material, $p^\star$.

$$\frac{\partial^2 p^\star}{\partial x^2} + \frac{\partial^2 p^\star}{\partial y^2} + \frac{\partial^2 p^\star}{\partial z^2} = 0 \tag{7}$$

Eqs. (1) and (2) are integrated with respect to (5), (6) boundary conditions.

$$u = -\frac{h_0^2}{\mu_1 \left(\frac{h}{h_0}\right)^Q M^2} \frac{\partial p}{\partial x} \left\{ \frac{1}{R_1^2 - R_2^2} \left(\frac{R_2^2 cosh \frac{R_1(2y-h)}{2l}}{cosh \frac{R_1 h}{2l}} \frac{R_1^2 cosh \frac{R_2(2y-h)}{2l}}{cosh \frac{R_2 h}{2l}} \right) + 1 \right\} \tag{8}$$

$$w = -\frac{h_0^2}{\mu_1 \left(\frac{h}{h_0}\right)^Q M^2} \frac{\partial p}{\partial z} \left\{ \frac{1}{R_1^2 - R_2^2} \left(\frac{R_2^2 cosh \frac{R_1(2y-h)}{2l}}{cosh \frac{R_1 h}{2l}} - \frac{R_1^2 cosh \frac{R_2(2y-h)}{2l}}{cosh \frac{R_2 h}{2l}} \right) + 1 \right\} \tag{9}$$

where, $M = B_0 h_0 \left(\frac{\sigma}{\mu}\right)^{\left(\frac{1}{2}\right)}$ is the Hartmann number.

$$R_1 = \left(\frac{1 + \sqrt{1 - 4l^2 M^2 / h_0^2}}{2} \right)^{(1/2)}, R_2 = \left(\frac{1 - \sqrt{1 - 4l^2 M^2 / h_0^2}}{2} \right)^{(1/2)}$$

Solving the Eq. (8) and (9) by applying the boundary condition (5), (6) and integrating throughout the film thickness h gives:

$$\frac{\partial^2 p}{\partial x^2} + \frac{\partial^2 p}{\partial z^2} = \frac{\mu_1 \left(\frac{h}{h_0}\right)^Q M^2 \frac{dh}{dt}}{h_0^2 \left(g(h,l,M) + \left(\frac{12\delta k}{1-\beta}\right) \right)} \tag{10}$$

where,

$$g(h,l,M)=\frac{2l}{R_1^2-R_2^2}\left(\frac{R_2^2}{R_1}tanh\frac{R_1h}{2l}-\frac{R_1^2}{R_2}tanh\frac{R_2h}{2l}\right)+h$$

The stochastic average of Eq. (10) is obtained by applying expectation operation on both sides with respect to $f(h_s)$, which takes the form.

$$\frac{\partial^2E(p)}{\partial x^2}+\frac{\partial^2E(p)}{\partial z^2}=\frac{\mu_1\left(\frac{h}{h_0}\right)^Q M^2\frac{dh}{dt}}{h_0^2\left(E(g(h,l,M))+\left(\frac{12\delta k}{1-\beta}\right)\right)} \tag{11}$$

Eq. (11) represents the average modified Reynolds equation for radial roughness pattern.

$$\frac{\partial^2E(p)}{\partial x^2}+\frac{\partial^2E(p)}{\partial z^2}=\frac{\mu_1\left(\frac{h}{h_0}\right)^Q M^2\frac{dh}{dt}}{\left[\frac{1}{h_0^2\left(E(g(h,l,M))+\left(\frac{12\delta k}{1-\beta}\right)\right)}\right]} \tag{12}$$

Eq. (12) represents the average modified Reynolds equation for azimuthal roughness pattern.

Combining the above equations gives

$$\frac{\partial^2p}{\partial x^2}+\frac{\partial^2p}{\partial z^2}=\frac{\mu_1\left(\frac{h}{h_0}\right)^Q M^2\frac{dh}{dt}}{h_0^2\left(G(h,l,M,c)+\left(\frac{12\delta k}{1-\beta}\right)\right)} \tag{13}$$

where,

$$G(h,l,M,c)=\begin{cases}E(g(h,l,M)) & \text{Radialroughness}\\ \left[\frac{1}{E(g(h,l,M))}\right]^{-1} & \text{Azimuthalroughness}\end{cases}$$

2.1 Annular plates

The flow is axisymmetric and the Eq. (13) reduces to:

$$\frac{1}{r}\frac{\partial}{\partial r}\left(r\frac{\partial p}{\partial r}\right)=\frac{\mu_1(\frac{h}{h_0})^Q M^2\frac{dh}{dt}}{h_0^2\left(G(h,l,M,c)+\left(\frac{12k\delta}{(1-\beta)}\right)\right)} \tag{14}$$

Solving (14) with the boundary conditions

$$P(a)=P(b)=0$$

the non-dimensional equation for annular plates pressure is obtained by:

$$P^\star=-\frac{h_0^3p}{\mu_1\left(\frac{dh}{dt}\right)(a^2-b^2)\pi}=\frac{(\frac{h}{h_0})^Q M^2}{4\pi G^\star(H^\star,l^\star,M,c)\left(\frac{12\Psi}{(1-\beta)}\right)}\left(\frac{logr^\star}{loga^\star}-\frac{r^{*2}}{a^{*2}}\right) \tag{15}$$

The expression for work load in non-dimensional form for annular plates is given by,

$$W^\star=-\frac{Wh_0^3}{\mu_1(\frac{dh}{dt})(a^2-b^2)^2\pi^2}=\frac{(\frac{h}{h_0})^Q M^2}{8\pi G^\star(H^\star,l^\star,M,c)\left(\frac{12\Psi}{(1-\beta)}\right)}\left(\frac{r^{*2}+1}{a^{*2}+1}-\frac{1}{loga^*}\right) \tag{16}$$

where,

$$G^\star(H^\star,l^\star,M,c)=h_0^2(G(h,l,M,c))$$
$$h^\star=\frac{h}{h_0}=H^*=h^*+h_s,$$
$$a^\star=\frac{a}{b},\Psi=\frac{k\delta}{h_0^3},l^\star=\left(\frac{2l}{h_0}\right),r^\star=\frac{r}{b}$$

2.2 Circular plates

The Eq. (13) is solved using the boundary conditions specific to circular plates, which are as follows:

$$P(a)=0\ and\ \left(\frac{\partial p}{\partial r}\right)_{r=0}=0$$

The following equation provides the dimensionless expression for pressure.

$$P^\star=-\frac{h_0^3p}{\mu_1(\frac{dh}{dt})a^2\pi}=\frac{(\frac{h}{h_0})^Q M^2[1-r^2]}{4\pi G^\star(H^\star,l^\star,M,c)+\left(\frac{12\Psi}{(1-\beta)}\right)} \tag{17}$$

The non-dimensional expression for work load for circular plates is given by:

$$W^\star=-\frac{Wh_0^3}{\mu_1(\frac{dh}{dt})a^4\pi^2}=\frac{(\frac{h}{h_0})^Q M^2}{8\pi G^\star(H^\star,l^\star,M,c)+\left(\frac{12\Psi}{(1-\beta)}\right)} \tag{18}$$

the radius of plates is represented by the parameter a.

2.3 Elliptic plates

The Eq. (13) is solved by using boundary conditions specific to elliptic plates as given in Eq. (19).

$$p(x_1,z_1)=0 \tag{19}$$

where,

$$\frac{x_1^2}{a^2}+\frac{z_1^2}{b^2}=1$$

The following equation represents the non-dimensional expression for the pressure distribution for elliptic plates.

$$P^\star=-\frac{h_0^3p}{\mu_1(\frac{dh}{dt})ab\pi}=\frac{(\frac{h}{h_0})^Q M^2a^\star}{2\pi(a^2+1)G^\star(H^\star,l^\star,M,c)+\left(\frac{12\Psi}{(1-\beta)}\right)} \tag{20}$$

the following equation provides the non-dimensional expression for the workload associated with elliptic plates.

$$W^\star=-\frac{Wh_0^3}{\mu_1(\frac{dh}{dt})a^2b^2\pi^2}=\frac{(\frac{h}{h_0})^Q M^2a^\star}{4\pi(a^2+1)G^\star(H^\star,l^\star,M,c)+\left(\frac{12\Psi}{(1-\beta)}\right)} \tag{21}$$

2.4 Triangular plates

Solving Eq. (13) with the boundary conditions

$$p(\bar{x},\bar{z})=0$$
$$(\bar{x}-a)(\bar{x}-\sqrt{3}\bar{z}+2a)(\bar{x}-\sqrt{3}\bar{z}+2a)=0$$

In the above equation, the parameter $2\sqrt{3}a$ denotes the length of the equilateral triangle.

The following equation provides the equation for pressure in non-dimensional form is given by:

$$P^{\star} = -\frac{h_0^3 p}{\mu_1(\frac{dh}{dt})3\sqrt{3}a^2} = \frac{(\frac{h}{h_0})^Q M^2}{9\sqrt{3}G^{\star}(H^{\star},l^{\star},M,c)+\left(\frac{12\Psi}{(1-\beta)}\right)} \times \left(1 - \frac{x}{a}\right)\left(1+\frac{\sqrt{3}z}{2a}+\frac{x}{2a}\right)\left(1-\frac{\sqrt{3}z}{2a}+\frac{x}{2a}\right) \quad (22)$$

the following equation provides the expression for workload in non-dimensional form.

$$W^{\star} = -\frac{Wh_0^3}{27\mu_1(\frac{dh}{dt})a^4} = \frac{\sqrt{3}(\frac{h}{h_0})^Q M^2 a^{\star}}{60G^{\star}(H^{\star},l^{\star},M,c)+\left(\frac{12\Psi}{(1-\beta)}\right)} \quad (23)$$

2.5 Rectangular plates

When the Eq. (13) is solved with boundary condition:

$$p\left(\pm\frac{a}{2},z\right) = 0$$
$$p\left(x,\pm\frac{b}{2}\right) = 0$$

the following equation provides the expression for pressure distribution in rectangular plates in non-dimensional form,

$$P^{\star} = -\frac{h_0^3 p}{\mu_1(\frac{dh}{dt})ab} = \frac{(\frac{h}{h_0})^Q M^2}{2a^{\star}G^{\star}(H^{\star},l^{\star},M,c)+\left(\frac{12\Psi}{(1-\beta)}\right)} \times \left\{\frac{1}{4}-\frac{z^2}{b^2}-\frac{8}{\pi^3}\sum_{n=1}^{\infty}\frac{(-1)^n cosh\frac{(2n+1)\pi x}{b} cosh\frac{(2n+1)\pi z}{b}}{(2n+1)^3 cosh\frac{(2n+1\pi a^{\star})}{2}}\right\} \quad (24)$$

The work load in non-dimensional form is given by:

$$W^{\star} = -\frac{Wh_0^3}{\mu_1(\frac{dh}{dt})a^2b^2} = \frac{(\frac{h}{h_0})^Q M^2}{\pi^4 a^{\star 2}G^{\star}(H^{\star},l^{\star},M,c)+\left(\frac{12\Psi}{(1-\beta)}\right)} \times \left[\frac{\pi^4 a^{\star}}{12}-\frac{16}{\pi}\sum_{n=1}^{\infty}\frac{tanh(\frac{2n+1}{2})\pi a^{\star}}{(2n+1)^5}\right] \quad (25)$$

In the above equation, a and b denote the sides of the rectangular plate. The values of the series solution in Eqs. (24) and (25) are computed up to n=100.

3. RESULTS AND DISCUSSIONS

This study delves into the exploration of squeeze film properties across different shapes under the influence of rough surface, magnetic field, and couple-stress. The analysis focuses on the effect of three dimensionless parameters (*c, M,* and $l^{\star}$) on the squeeze film, with *c* representing the roughness parameter, *M* is the Hartmann number and the existence of polar additives in the lubricant leads to the emergence of the parameter $l^{\star}$, which can be thought of as the chain length of the polar additives within the fluid. $l^{\star}$ influences the way in which the fluid interacts with the bearing geometry.

For all the shapes analyzed, the general equation for the load is as follows:

$$W^{\star} = \frac{Wh_0^3}{\mu(\frac{dh}{dt})\bar{A}^2} = S_f K$$

with S_f representing the shape-factor provided by Table 1, $\bar{A}$ symbolizing the key area of the plate, and $K = \frac{M^2}{G^{\star}(H^{\star},l^{\star},M,c)+\left(\frac{12\Psi}{(1-\beta)}\right)}$ a parameter that considers the impacts of couple-stresses, hydro-magnetic effects, and surface roughness.

Table 2 displays the changes in the non-dimensional workload, $W^{\star}$, as a result of the variation in the couple-stress parameter $l^{\star}$, roughness parameter *c*, and magnetic parameter*M*. It can be observed that the use of couple-stress fluid in conjunction with magnetic field and surface roughness significantly improves the workload compared to a smooth surface Fathima et al. [8] and traditional non-conducting Newtonian fluids. The reason for this is that the externally applied magnetic field, which is perpendicular to the flow, causes a reduction in the velocity of the fluid in the film region. Additionally, surface roughness minimizes sideways fluid leakage and slows down the fluid velocity, thereby retaining a large amount of fluid in the fluid film region, resulting in a substantial pressure distribution.

Table 3 showcases the variation of non-dimensional workload with variation in viscosity with porous and non-porous cases. The data suggests that, for both non-porous and porous cases, the workload increases as the viscosity variation parameter Q increases. However, it is observed that the workload of the non-porous case is higher than that of the porous case.

The impact of plate shape on the workload is displayed in Figure 2. From the graph it is observed that workload increases as Hartmann number increases with surface roughness *c.* The variation of workload with changes in viscosity is shown in Figure 4, it is noted that load increasing as Q increases. The results of the study show that circular plates, when lubricated with couple-stress fluid and subjected to surface roughness in the presence of a transverse magnetic field, perform better in terms of squeeze film performance compared to the conventional scenario of using a non-conducting Newtonian fluid and a smooth surface. The impact of plate shape with porosity on the workload is displayed in Figure 3 and the variation of workload with viscosity variation and porosity are shown in Figure 5. Among all geometries, lubricated with couple-stress fluid with surface roughness in the presence of a transverse magnetic field exhibit lower squeeze film performance compared to the non-porous case.

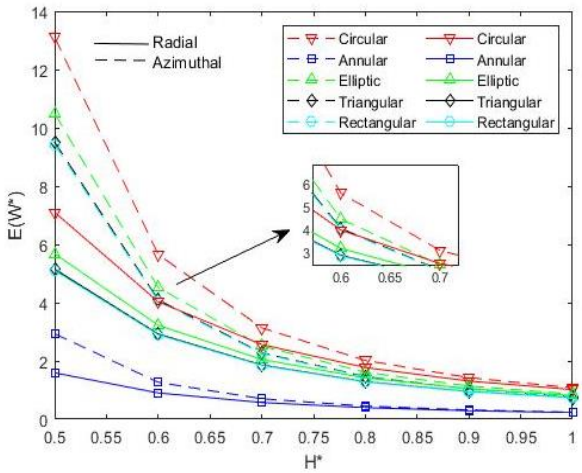

Figure 2. Plot of non-dimensional workload $W^{\star}$ and $H^{\star}$ for various geometries with *c=0.3*, $l^{\star} = 0.3$, *M=3*, $a^{\star} = 2$

Table 1. Shape-factor of various plates

Different Geometry	Characteristics Area $\overline{A}$	Shape-factor S_f	S_f at $a^\star = 2$
Annular	$(a^2 - b^2)\pi$	$\frac{1}{8\pi}\left(\frac{a^{*2}+1}{a^{*2}-1} - \frac{1}{log a^*}\right)$	0.0089116
Circular	πa^2	$\frac{1}{8\pi}$	0.0397880
Elliptic	πab	$\frac{1}{4\pi}\left(\frac{a^\star}{a^{\star 2}+1}\right)$	0.0318310
Triangular	$3\sqrt{3}a^2$	$\frac{\sqrt{3}}{60}$	0.0288680
Rectangular	ab	$\frac{1}{\pi^4 a^{\star 2}}\left(\frac{\pi^4 a^\star}{12} - \frac{16}{\pi}\sum_{n=1}^{\infty}\frac{tanh(\frac{2n+1}{2})\pi a^\star}{(2n+1)^5}\right)$	0.0285850

Table 2. Non-dimensional $W^\star$ work load for diverse values of *M* with roughness *c* and $l^\star$ at $a^\star = 2$ and $H^\star = 0.3$

Different Geometries Work Load	M	Ψ=0, Q =0, C=0.3		C=0.0 [17]
		Azimuthal	Radial	M
Circular	0	78.1304	15.5817	62.0957
	1	78.2699	15.7651	62.2591
	2	78.6886	16.31	62.7481
	3	79.3864	17.2014	63.563
Elliptic	0	62.5043	12.4653	49.6765
	1	62.6159	12.6121	49.8073
	2	62.9509	13.048	50.1985
	3	63.5091	13.7611	50.8504
Triangular	0	56.6851	11.3048	45.0516
	1	56.7864	11.4379	45.1702
	2	57.0901	11.8332	45.525
	3	57.5964	12.4799	46.1162
Rectangular	0	56.1304	11.1942	44.6111
	1	56.2306	11.326	44.7285
	2	56.5314	11.7174	45.0798
	3	57.0327	12.3578	45.6652
Annular	0	17.4989	3.4898	13.9077
	1	17.5302	3.5309	13.9443
	2	17.624	3.65298	14.0538
	3	17.7803	3.8526	14.2363

Table 3. The non-dimensional workload variation with height is shown for distinct values of the viscosity variation parameter *Q*, with *M=3*, *c=0.3*, $l^\star = 0.3$, and $H^\star = 0.5$ at $a^\star = 2$

Different Plates		C=0.3, Ψ=0.0		C=0.3, Ψ =0.001	
	Q	Azimuthal	Radial	Azimuthal	Radial
Circular	0	6.5521	3.5499	3.3663	2.6494
	0.1	9.3040	4.7899	4.5420	3.5748
	0.2	13.2117	6.4629	6.1285	4.8235
	0.3	18.7606	8.7203	8.2691	6.5082
Elliptic	0	5.2417	2.8400	2.6930	2.1196
	0.1	7.0725	3.8319	3.6336	2.8599
	0.2	9.5429	13.0480	4.9028	3.8588
	0.3	12.8760	6.9762	6.6153	5.2066
Triangular	0	4.7537	2.5756	2.4423	1.9222
	0.1	6.4141	3.4752	3.2953	2.5936
	0.2	8.6544	4.6890	4.4463	3.4995
	0.3	11.6772	6.3267	5.9994	4.7219
Rectangular	0	4.7072	2.5504	2.4184	1.9034
	0.1	6.3513	3.4411	3.2631	2.5682
	0.2	8.5697	4.6431	4.4028	3.4653
	0.3	11.5630	6.2648	5.9407	4.6756
Annular	0	1.4675	0.7951	0.7539	0.5934
	0.1	1.9801	1.0728	1.0173	0.8007
	0.2	2.6717	1.4475	1.3726	1.0803
	0.3	3.6048	1.9531	1.8520	1.4577

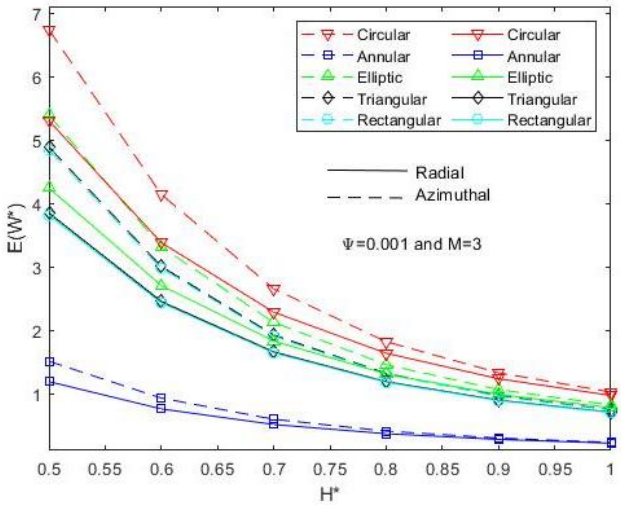

Figure 3. Variation in non-dimensional workload $W^{\star}$ and $H^{\star}$ for various geometries with c=0.3, $\Psi = 0.001$, $l^{\star} = 0.3$, M=3, $a^{\star} = 2$

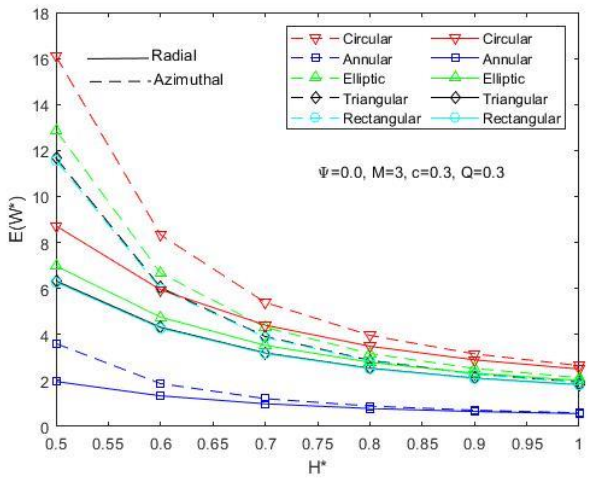

Figure 4. Plot of non-dimensional workload $W^{\star}$ and $H^{\star}$ for various geometries with Q=0.3, $l^{\star} = 0.3$, c=0.3, M=3, $a^{\star} = 2$

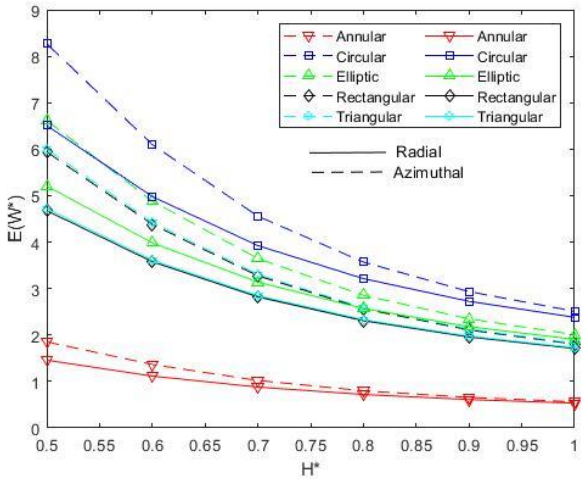

Figure 5. Plot of non-dimensional workload $W^{\star}$ and $H^{\star}$ for various geometries with $\Psi = 0.001$, Q=0.3, c=0.3, $l^{\star} = 0.3$, M=3, $a^{\star} = 2$

4. CONCLUSION

This article delves into the analysis of the performance of various geometries under the effect of surface roughness, MHD and couple-stress fluid. The results show that the workload, with its sensitivity to surface roughness and viscosity variation, increases as the magnetic parameter M, roughness parameter c, and couple-stress parameter $l^{\star}$ increase. It's noteworthy that the non-dimensional workload depends solely on the shape-factor S_f. Therefore, circular plates demonstrate the greatest work load compared to other plate shapes, as indicated in Table 2. Furthermore, Table 3 shows that the work load decreases in the presence of porosity for all plate geometries.

REFERENCES

[1] Ariman, T., Turk, M.A., Sylvester, N.D. (1973). Micro continuum fluid mechanics-a review. International Journal of Engineering Science, 11(8): 905-930. https://doi.org/10.1016/0020-7225(73)90038-4

[2] Ariman, T., Turk, M.A., Sylvester, N.D. (1974). Application of microcontinuum fluid mechanics. International Journal of Engineering Science, 12(4): 273-287. https://doi.org/10.1016/0020-7225(74)90059-7

[3] Stokes, V.K. (1966). Couple-stresses in fluids. Physics of Fluids, 9: 1709-1715. https://doi.org/10.1063/1.1761925

[4] Lin, J.R. (1998). Squeeze film characteristics of finite journal bearings: Couple stress fluid model. Tribology International, 31(4): 201-207. https://doi.org/10.1016/S0301-679X(98)00022-X

[5] Naduvinamani, N.B., Fathima, S.T., Hiremath, P.S. (2003). Lubricant additives effects on the squeeze film lubrication between anisotropic porous rectangular plates. Industrial Lubrication and Tribology, 55(4): 184-192. http://dx.doi.org/10.1108/00368790310480371

[6] Naduvinamani, N.B., Patil, S.B. (2009). Numerical solution of finite modified reynolds equation for couple stresses squeeze film lubrication of porous journal bearings. Computers and Structures, 87(21-22): 1287-1295. https://doi.org/10.1016/j.compstruc.2009.08.004

[7] Ramanaiah, G. (1979). Squeeze films between finite plates lubricated by fluids with couple stress. Wear, 54(2): 315-320. https://doi.org/10.1016/0043-1648(79)90123-6

[8] Bujurke, N.M., Jayaraman, G. (1982). The influence of couple-stresses in squeeze films. International Journal of Mechanical Sciences, 24(6): 369-376. https://doi.org/10.1016/0020-7403(82)90070-4

[9] Tzeng, S.T., Saibel, E. (1967). Surface roughness effect on slider bearing lubrication. Asle Transactions, 10(3): 334-348. https://doi.org/10.1080/05698196708972191

[10] Christensen, H. (1969). Stochastic models for hydrodynamic lubrication of rough surfaces. Proceedings of the Institution of Mechanical Engineers, 184(1): 1013-1026. https://doi.org/10.1243/PIME_PROC_1969_184_074_02

[11] Christensen, H., Tonder, K.C. (1969). Tribology of rough surfaces: Stochastic models of hydrodynamic lubrication. Sintef Report, 10(69): 18.

[12] Christensen, H., Tønder, K. (1969). Parametric study and comparison of lubrication models. SINTEF, Technical Report No. SINTEF 22/69-18.
[13] Christensen, H., Tonder, K.C. (1971). The hydrodynamic lubrication of rough bearing surfaces of finite width. Journal of Lubrication Technology, 93(3): 324-329. https://doi.org/10.1115/1.3451579
[14] Naduvinamani, N.B., Hiremath, P.S., Gurubasavaraj, G. (2005). Effect of surface roughness on the couple-stress squeezes film between a sphere and a flat plate. Tribology International, 38(5): 451-458. https://doi.org/10.1016/j.triboint.2004.09.001
[15] Rajani, C.B., Hanumagowda, B.N., Shigehalli, V.S. (2018). Effects of surface roughness on conical squeeze film bearings with micropolar fluid. Journal of Physics: Conference Series, 1000(1): 012079. https://doi.org/10.1088/1742-6596/1000/1/012079
[16] Naduvinamani, N.B., Kadadi, A.K. (2013). Effect of viscosity variation on the micropolar fluid squeeze film lubrication of a short journal bearing. Advances in Tribology, 2013: 743987. https://doi.org/10.1155/2013/743987
[17] Fathima, S.T., Naduvinamani, N.B., Hanumagowda, B.N., Kumar, J.S. (2015). Modified reynolds equation for different types of finite plates with the combined effect of MHD and couple stresses. Tribology Transactions, 58(4): 660-667. https://doi.org/10.1080/10402004.2014.981906

NOMENCLATURE

a, b	Dimensions of the bearing (m)
B_0	Applied magnetic field
Q	Viscosity variation parameter
M	Hartmann number
$H^{\star}$	Dimensionless film thickness
h	Film thickness (m)
h_0	Minimum film thickness (m)
h_s	Stochastic variable
l	$= \sqrt{\frac{\eta}{\mu}}$ Couple stress parameter
$l^{\star}$	$= \left(\frac{2l}{h_0}\right)$ Non-dimensional couple-stress parameter

Greek symbols

β	percolation parameter
η	Material constant characterizing couple stress
σ	Electrical conductivity (S/m)
μ	dynamic viscosity $(\mathrm{Ns/m^2})$
μ_1	known viscosity at minimum film thickness.
Ψ	permeability parameter